Supporting Information for:

Linking Optical Spectra to Free Charges in Donor/Acceptor Heterojunctions: Cross-Correlation of Transient Microwave and Optical Spectroscopy

Hyun Suk Kang,[a] Samuel Peurifoy,[b] Boyuan Zhang,[b] Andrew J. Ferguson,[a] Obadiah G. Reid,[a,c] Colin Nuckolls,[b] Jeffrey L. Blackburn[a*]

[a]National Renewable Energy Laboratory, Golden, Colorado 80401, United States
[b]Department of Chemistry, Columbia University, New York, New York 10027, United States
[c]Renewable and Sustainable Energy Institute, University of Colorado Boulder, Boulder, Colorado 80303, United States

Table of Contents

Topic **Page**
1. Experimental Methods……S1-S3
2. Absorption spectra of neat films and bilayers of s-SWCNTs and **Trip-hPDI2**/C_{60} ……....S4
3. TA spectra/kinetics of SWCNT neat film and hPDI2-pyr-hPDI2 bilayer……S5
4. TA kinetics of s-SWCNTs/electron acceptors bilayers …… S5-S7
5. TA and TRMC kinetics of other SWCNTs bilayers ……..……..S8
6. Convolution of TA dynamics with a 4 ns instrument response function (IRF) …….... S9
7. Kinetic simulations comparing fs vs. ns excitation pulses …….……S10-S11
8. Supporting Information References……....….S12

1. Experimental Methods

Syntheses of PDI-based electron acceptors. Syntheses of **hPDI2-pyr-hPDI2** and **Trip-hPDI2** was described previously.[1, 2]

Film Preparation. SWCNTs for preparing enriched (6,5) and (7,5) s-SWCNT samples were purchased from CHASM (CoMoCAT SG65i). The wrapping polymers, poly-[(9,9-dioctylfluorenyl-2,7-diyl)-*alt*-*co*-(6,60-[2,20-bipyridine])] (PFO-bpy) and poly-[(9,9-dioctylfluorenyl-2,7-diyl)] (PFO) were purchased from American Dye Source and Solaris, respectively. To extract pure (6,5) or (7,5) s-SWCNTs from SG65i, SWCNTs were first mixed with PFO-bpy or PFO in toluene, respectively, at a mass loading (mg/mL) ratio of 1:4 or 1:3 (SWCNTs:polymer), where the SWCNT mass in all cases was 1 mg/mL. Dispersion was achieved by tip-sonication for 15 minutes at 40 % intensity (Cole-Palmer CPX 750, ½" tip) in a bath of cool (~18 °C) flowing water. The tip-sonicated dispersions in toluene were immediately centrifuged at 20 °C and 13200 rpm for 5 minutes (Beckman Coulter L-100 XP ultracentrifuge, SW-32 Ti rotor).

The supernatant, containing PFO-bpy-wrapped (6,5) SWCNTs or PFO-wrapped (7,5) SWCNTs, and excess polymer in both cases, was separated from the pellet by pipette. These supernatants were then centrifuged at 20 °C and 24100 rpm for 20 hours to remove excess polymer. The pellet, containing (6,5)/PFO-bpy or (7,5)/PFO SWCNTs, was separated from the supernatant of excess polymer. This long centrifuge process was repeated for the re-dispersed pellet in toluene to arrive a ~1:1 mass ratio of s-SWCNTs and corresponding polymer. The pellet was then re-dispersed in toluene in a heated ultrasonic bath for more than an hour to yield a homogeneous s-SWCNT ink.

Each s-SWCNT ink was spray-coated onto clean quartz substrates. Before spraying, the substrates were rinsed by acetone and isopropyl alcohol (IPA) and treated by O_3 plasma by 10 minutes. The s-SWCNT ink spray deposition process was described previously.[3] All SWCNT films were deposited and processed in air and the SWCNT network homogeneously covers the entire quartz substrate. After initial deposition, the s-SWCNT film was soaked in toluene to remove excess toluene and ensure good electronic coupling between SWCNT bundles. Despite the presence of some residual wrapping polymer, even after this toluene soaking step, the s-SWCNT networks prepared in this manner show large conductivities when doped with charge carriers via molecular redox dopants.[4] This ensures that the TA and TRMC measurements discussed here are performed on well-coupled networks of highly conductive SWCNTs.

The PDI-based electron acceptors were then deposited onto both clean quartz substrates for neat films and s-SWCNT films for bilayers. Each acceptor solution in chloroform (**hPDI2-pyr-hPDI2**: 2.5 mg/mL, **Trip-hPDI2**: 3.3 mg/mL) was spin-coated (in air) at 1000 rpm for 1 min by dispensing 100 µL solution onto the substrate and then spinning. C_{60} (~90 nm) was deposited onto both clean quartz substrates for neat films and s-SWCNT films for bilayers *via* thermal deposition at a pressure of $<1 \times 10^{-6}$ Torr and a deposition rate of 0.5 Å/s.

Static and Transient Absorption. To ensure that all films were in an inert atmosphere during all absorption and TA measurements, all samples on quartz substrates were introduced into a nitrogen glovebox and inserted into an air-free holder (Thorlabs Ø2in Tubes without External Threads). No additional treatments (e.g. annealing) were performed on the samples once in the glovebox before loading into the air-free holder. The ground-state absorption spectra of neat films and bilayers of s-SWCNTs and PDI-based acceptors were measured on a Varian Cary 5000 spectrophotometer in the wavelength range of 200-1500 nm with baseline correction. Those of neat films and bilayers

from C_{60} were measured in the Integrating Sphere (UV-Vis-NIR External Diffuse Reflectance Accessories (DRA 2500)) on a Varian Cary 5000 spectrophotometer to subtract strong beam scattering by the 90 nm C_{60} layer to obtain the true absorption spectra of C_{60}-related samples. The s-SWCNT film thickness was estimated using its S_{11} peak optical density at 1000 for (6,5) or 1050 nm for (7,5) SWCNT,[5, 6] and is estimated to be ca. 10 nm for the films studied here. The configurations of ultrafast pump-probe time-resolved spectroscopic measurement system (Ultrafast Systems) to measure transient absorption spectra and dynamics of the films were described previously.[3] To probe hole transfer, the excitation pump pulse wavelengths used to excite PDI-based acceptors were selected to also avoid polymer excitation. Excitation wavelengths of 415 and 450 nm were used for the PDI-based heterojunctions containing PFO-bpy (6,5) and PFO (7,5), respectively. For C_{60} excitation, only 450 nm excitation was utilized. To probe electron transfer, 1000 nm and 1050 nm were selected for (6,5) SWCNT and (7,5) SWCNT-related films, respectively, to directly excite the samples at the s-SWCNT S_{11} excitonic transition. The pump pulse energies for the bilayers were $2.03 \times 10^{12} – 1.29 \times 10^{13}$ photons·pulse^{-1}·cm^{-2} at 415 nm, $3.13 \times 10^{12} – 2.29 \times 10^{13}$ photons·pulse^{-1}·cm^{-2} at 450 nm, $6.96 \times 10^{12} – 2.66 \times 10^{13}$ photons·pulse^{-1}·cm^{-2} at 1000 nm, and $1.65 \times 10^{12} – 1.32 \times 10^{13}$ photons·pulse^{-1}·cm^{-2} at 1050 nm.

Time-resolved Microwave Conductivity. All samples on quartz substrates were placed in an X-band (9.9 GHz) microwave waveguide in a nitrogen glovebox to ensure an inert atmosphere. As with static and transient absorption experiments, no additional treatments (e.g. annealing) were performed on the samples once in the glovebox before loading into the air-free holder. The structure of X-band waveguide and the instrument settings of TRMC measurements are described in detail elsewhere.[7] The entire sample area (~2 cm^2) was photoexcited with ~4 ns light pulses (30 Hz repetition rate) of tunable wavelength emanating from a Nd:YAG-pumped optical paramagnetic oscillator (OPO) attenuated with various combinations of neutral density filters. Then, time-dependent changes in the microwave probe power were measured with a calibrated Schottky barrier diode, and an oscilloscope with sub-ns resolution tracked the transient behavior of changes in microwave power. The photoconductance dynamics of bilayer films were measured in two different TRMC configurations: “cavity” and “open-cell” configurations. For the “cavity” configuration, a metal iris was inserted into the microwave waveguide to create a resonant microwave cavity to enhance signal at the expense of inferior time response. For the “open-cell”

configuration, the iris was removed from the waveguide to deduce the photoconductance dynamics with the full temporal resolution afforded by the ns scale optical pump. Even though the signal intensities were substantially lower than those from the cavity configuration, the open-cell signals measured here were sufficiently strong so that the photoconductance dynamics could be compared to the TA dynamics. Both configurations were employed to extract the saturated charge yield-mobility product values for each film, deducing the hole mobility values of s-SWCNTs in each bilayer. The K-factor values, used herein for the hole mobility calculation, are 24000 for the "cavity" configuration and 630 for the "open cell" configuration.[7] Since each configuration has potential drawbacks with respect to instrument time response and signal-to-noise ratio, respectively, yield-mobility product values from both configurations were averaged for better accuracy.

2. Absorption spectra of neat films and bilayers of s-SWCNTs and Trip-hPDI2/C_{60}

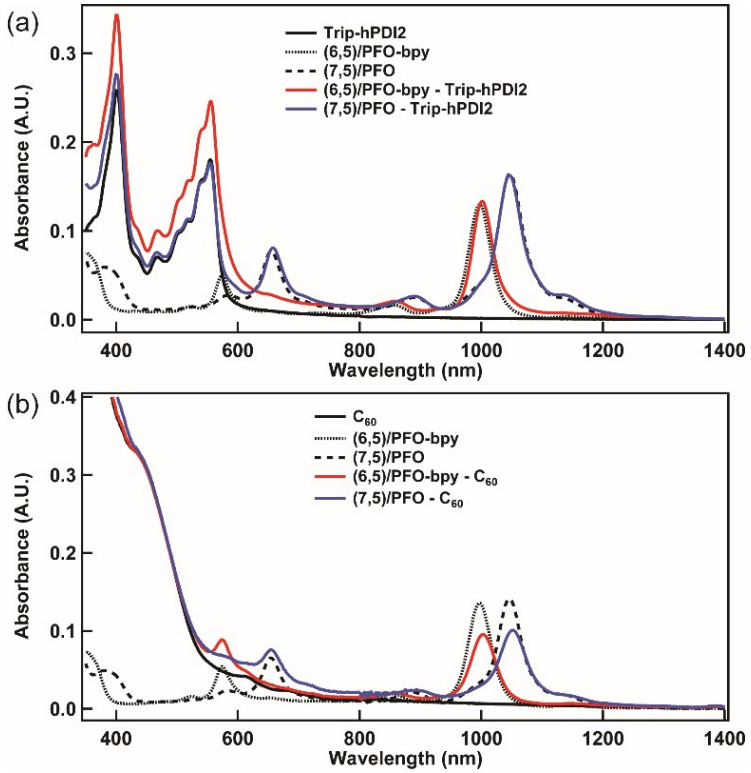

Figure S1. Ground-state absorption spectra of the bilayers and neat films of SWCNT and (a) **Trip-hPDI2**, (b) C_{60}. (black: electron acceptor neat film, dotted: (6,5) SWCNT neat film, dashed: (7,5) SWCNT neat film, red: (6,5) SWCNT – electron acceptor bilayer, blue: (7,5) SWCNT – electron acceptor bilayer)

3. TA spectra/kinetics of SWCNT neat film and hPDI2-pyr-hPDI2 bilayer

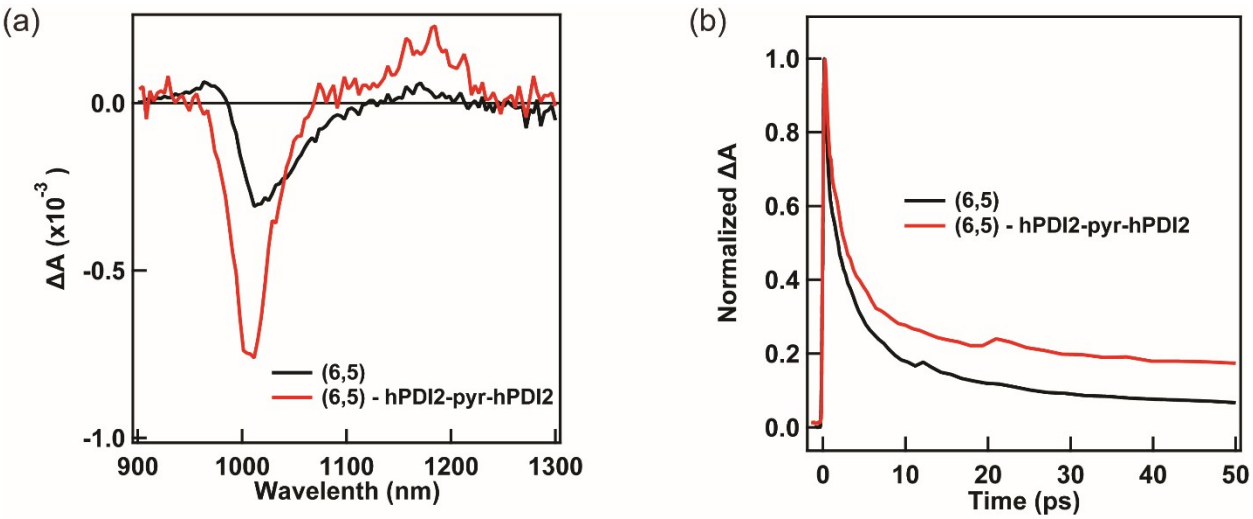

Figure S2. (a) TA spectra at 100 ps pump-probe delay and (b) TA kinetics of (6,5) SWCNT neat film and (6,5) SWCNT – **hPDI2-pyr-hPDI2** bilayer.

4. TA kinetics of s-SWCNTs/electron acceptors bilayers

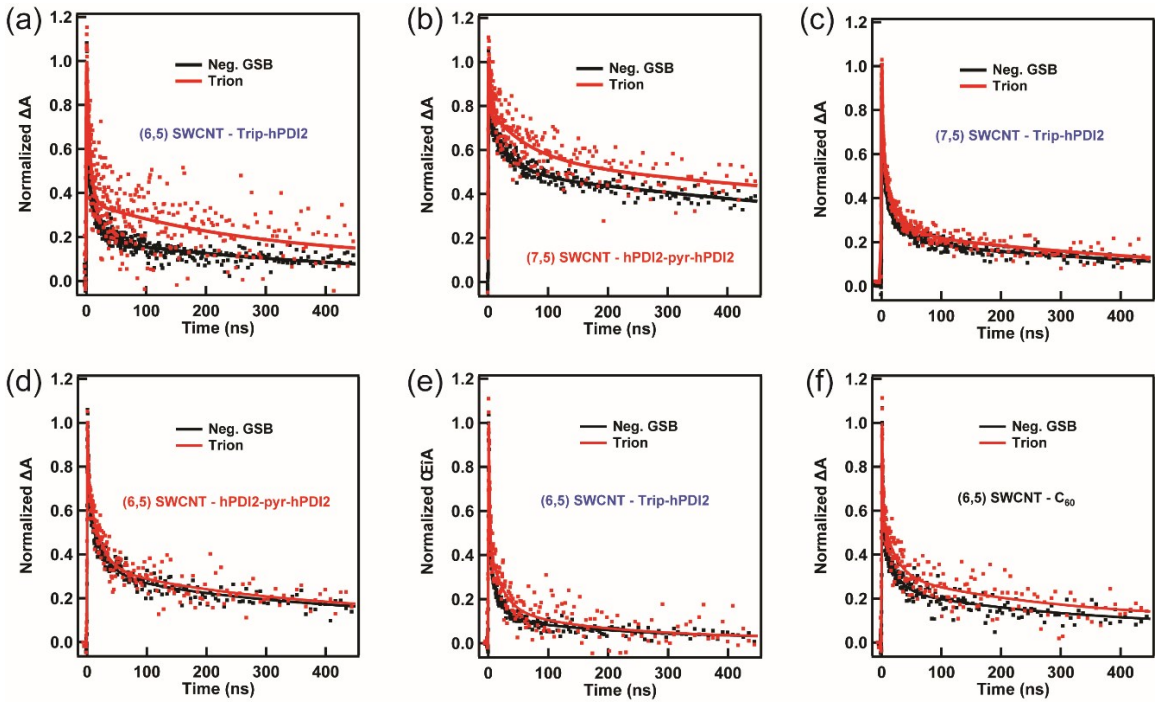

Figure S3. Normalized S_{11} ground state bleaching (GSB) and trion induced absorption (X^+) TA kinetic profiles of (a) (6,5) SWCNT – **Trip-hPDI2**, (b) (7,5) SWCNT – **hPDI2-pyr-hPDI2**, (c) (7,5) SWCNT – **Trip-hPDI2** for hole transfer and (d) (6,5) SWCNT – **hPDI2-pyr-hPDI2**, (e) (6,5) SWCNT – **Trip-hPDI2**, (f) (6,5) SWCNT – C_{60} for electron transfer up to 450 ns.

Kinetic profile comparisons for SWCNT – C_{60} hole transfer and (7,5) SWCNT – electron acceptors electron transfer are not shown here due to unknown long-living feature at S_{11} GSB and cutoff S_{11} GSB features by probe laser ND filter, respectively (Figure S3). S_{11} GSB features for (7,5) SWCNT – PDI acceptors hole transfer were obtained from the blue edge of cutoff S_{11} GSB main bands, while those for electron transfer were blocked by strong pump laser scattering.

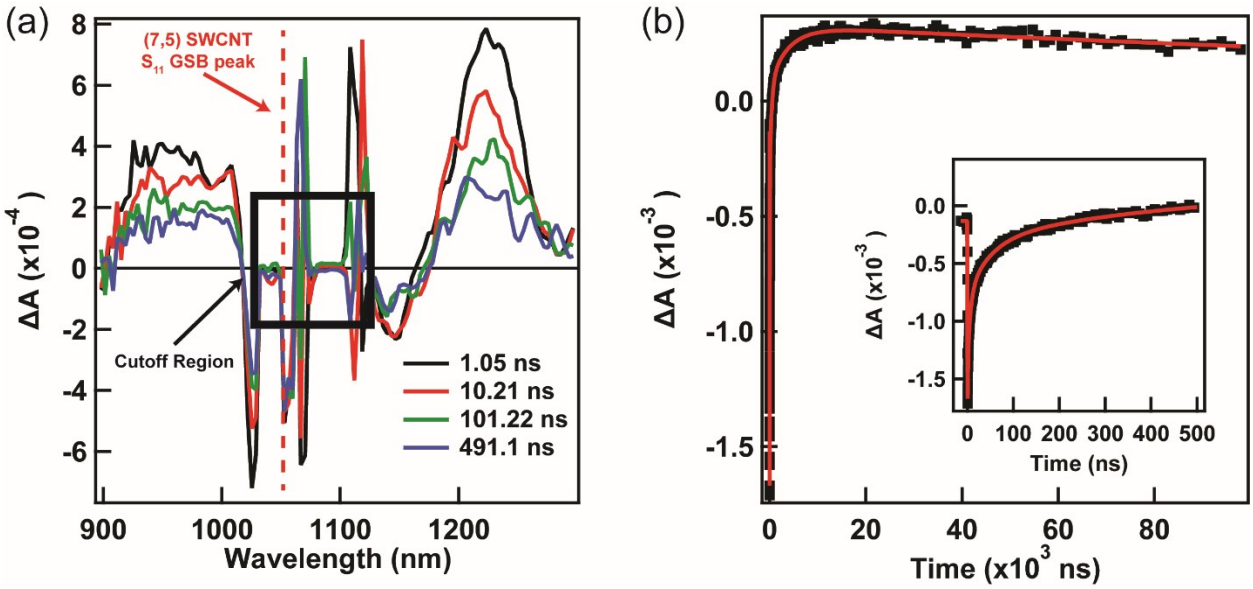

Figure S4. (a) Transient absorption profile of (7,5) SWCNT – **hPDI2-pyr-hPDI2**, excited at 450 nm. The S_{11} GSB peak wavelength is 1050 nm, and it is within the cutoff wavelength range by ND filter, indicated by black square in the graph. (b) Transient absorption kinetic profile of (6,5) SWCNT – C_{60}, excited at 450 nm. From around 500 ns, the induced absorption band arises up to 15 μs and then slowly decays beyond 100 μs.

Table S1. S_{11} GSB TA kinetic features of SWCNT – electron acceptors bilayers.

Hole Transfer			
(6,5) SWCNT – hPDI2-pyr-hPDI2		**(6,5) SWCNT – Trip-hPDI2**	
Time (ns)	Amplitude (relative)	Time (ns)	Amplitude (relative)
0.84 ± 0.085	0.30	0.74 ± 0.1	0.50
7.3 ± 0.52	0.20	6.78 ± 0.66	0.30
65.9 ± 5.28	0.16	55.8 ± 10.4	0.13
1846 ± 156	0.34	763.1 ± 262	0.07
(7,5) SWCNT – hPDI2-pyr-hPDI2		**(7,5) SWCNT – Trip-hPDI2**	
Time (ns)	Amplitude (relative)	Time (ns)	Amplitude (relative)
2.01 ± 0.24	0.34	0.49 ± 0.11	0.50
35.2 ± 4.11	0.21	4.73 ± 0.65	0.25
1450 ± 160	0.45	30.9 ± 5.38	0.12
		749.04 ± 93.4	0.13

Electron Transfer					
(6,5) SWCNT – hPDI2-pyr-hPDI2		**(6,5) SWCNT – Trip-hPDI2**		**(6,5) SWCNT – C_{60}**	
Time (ns)	Amplitude (relative)	Time (ns)	Amplitude (relative)	Time (ns)	Amplitude (relative)
2.03 ± 0.22	0.46	1.33 ± 0.073	0.67	1.19 ± 0.13	0.61
24.3 ± 2.92	0.27	14.1 ± 1.12	0.24	19.6 ± 2.84	0.20
325.7 ± 43.1	0.17	202.3 ± 28.7	0.07	303.6 ± 51.5	0.13
7861 ± 1080	0.10	13233 ± 5460	0.02	7697 ± 2050	0.06

5. TA and TRMC kinetics of other SWCNTs bilayers

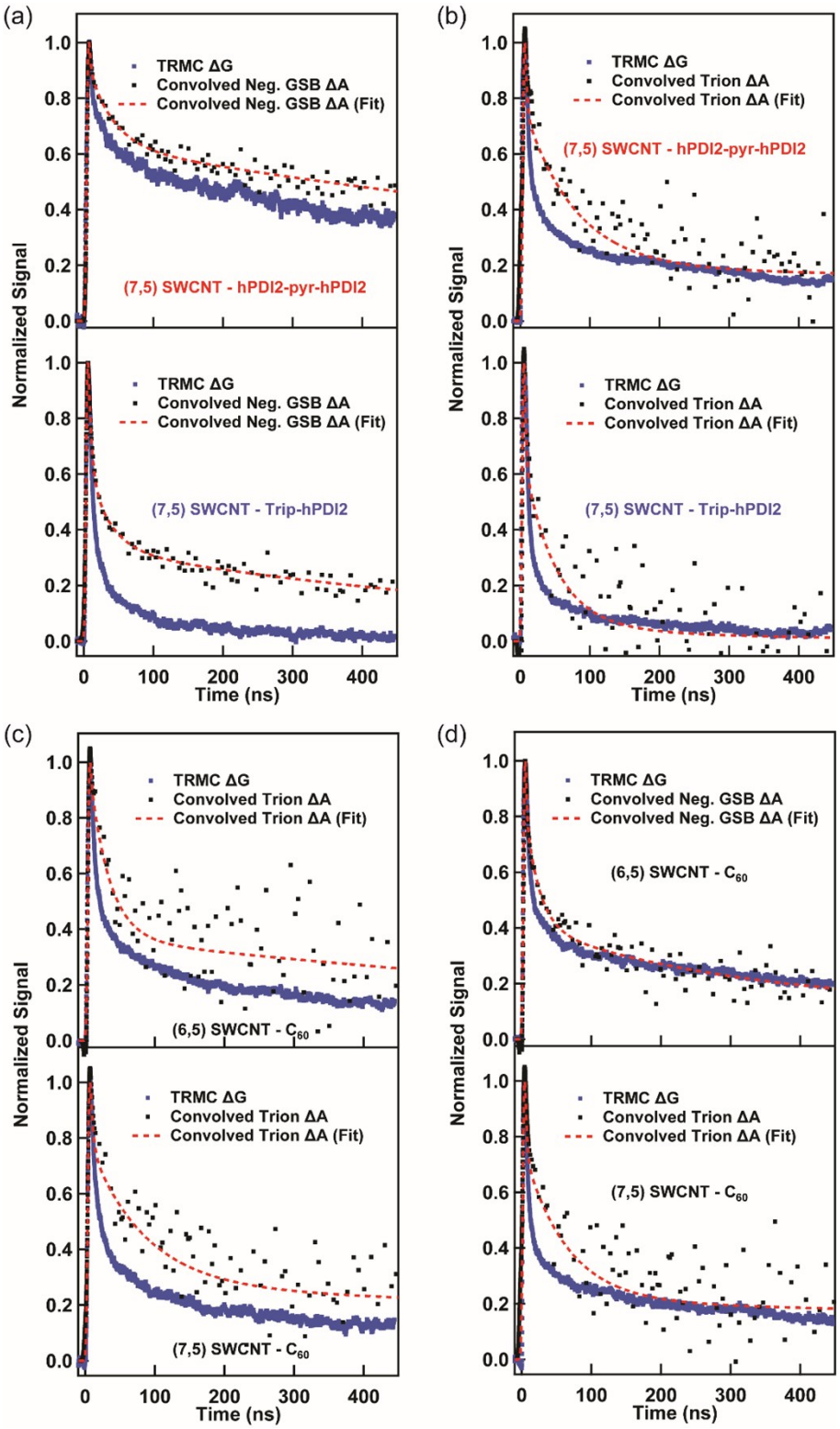

Figure S5. Comparison of normalized TA and TRMC kinetic profiles of (7,5) SWCNT – PDI acceptors bilayers for (a) hole transfer* and (b) electron transfer, and SWCNT – C_{60} bilayers for (c) hole transfer and (d) electron transfer.

For SWCNT – C_{60} hole transfer and (7,5) SWCNT – electron acceptors electron transfer, trion kinetic profiles were used since S_{11} GSB features could not be used (Vide Supra). Considered significantly lower signal-to-noise ratios for trion kinetic profiles, the comparisons between convolved trion (fitted) and TRMC kinetic profiles have nicely matched within error range. * (7,5) SWCNT GSB features in hole transfer were obtained at 1020 nm (Figure S2 – vide supra). The profile mismatch at (7,5) SWCNT – **Trip-hPDI2** indicates significant charge traps at the heterojunction, and the details will be examined in future.

6. Convolution of TA dynamics with a 4 ns instrument response function (IRF)

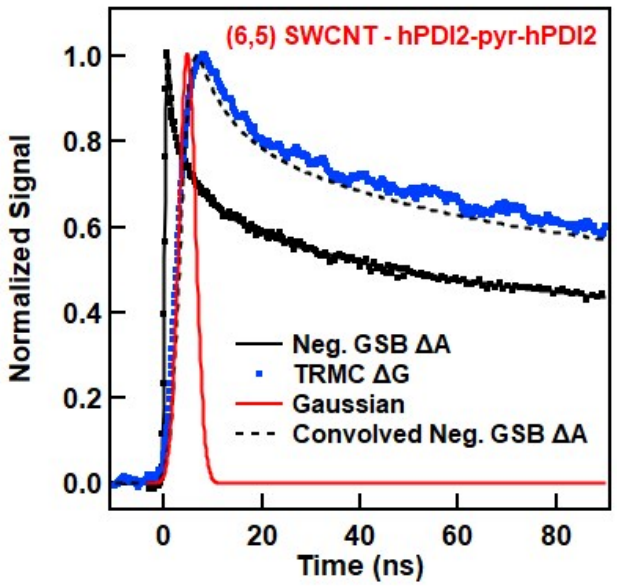

Figure S6. Comparison of normalized S_{11} GSB TA (black) and TRMC (blue) kinetic profiles of (6,5) SWCNT – **hPDI2-pyr-hPDI2** for hole transfer, Gaussian IRF of 4 ns (red), and reconvolved S_{11} GSB TA kinetic profiles by Gaussian IRF of 4 ns.

7. Kinetic simulations comparing fs vs. ns excitation

We use a simple kinetic simulation to show that for this excitation fluence, it is unlikely that second-order ECA or EEA processes would influence our results substantially. To do this we employed the following coupled differential equations:

$$\frac{d[E]}{dt} = N_0 g(t) - k_r - k_{CT}[E] - k_{EEA}[E]^2 - k_{ECA}[E][C]$$

$$\frac{d[C]}{dt} = k_{CT}[E]$$

Where $[E]$ is the concentration of excitons, $N_0$is the excitation density, $g(t)$ is the gaussian laser pulse envelope, k_r is the recombination rate constant of excitons, k_{CT} is the effective charge transfer rate constant, k_{EEA} is the exciton-exciton annihilation rate constant, k_{ECA} is the exciton-charge annihilation rate constant, and $[C]$ is the concentration of charges. Table S2 shows the chosen rate constants. We find that varying the laser pulse width from 265 fs to 5 ns (or experimental values) has only a marginal influence of the estimated charge yield. With these parameters, the charge yield for the 5 ns pulse is 45%, while for the 100 fs pulse it is 37.5%. This is fully consistent with the near-linear dependance we see of the TA and TRMC signals at this fluence, and is not a large enough difference to substantially influence the relative recombination dynamics in the two experiments.

parameter	value	unit
N_0	$1x10^{17}$	cm^{-3}
k_r	$1x10^{10}$	s^{-1}
k_{CT}	$1x10^{10}$	s^{-1}
k_{EEA}	$1x10^{-7}$	cm^3s^{-1}
k_{ECA}	$1x10^{-7}$	cm^3s^{-1}

Table S2) Rate constants used to estimate the influence of laser pulse width on the yield of charges in TA vs. TRMC experiments.

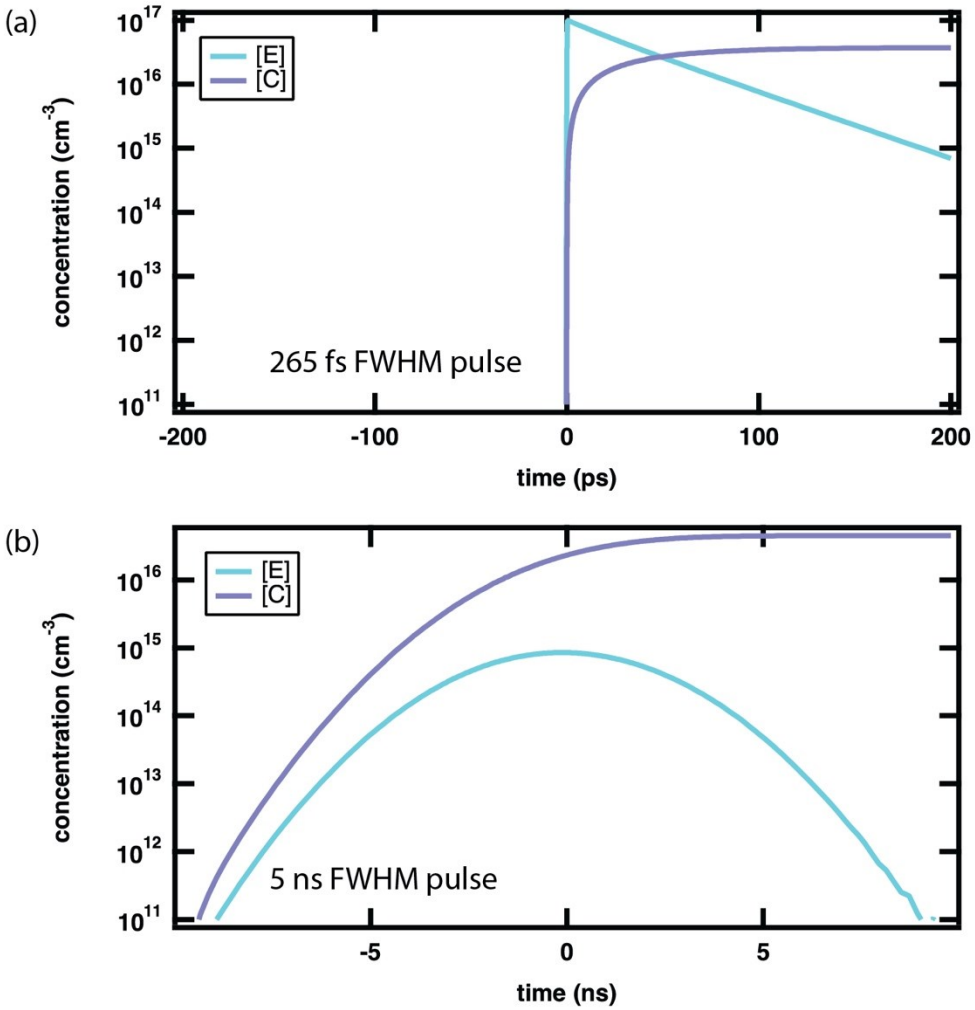

Figure S7) *Kinetic simulation results for exciton (purple) and charge (blue) concentration as a function of time, comparing (a) ~265 fs FWHM laser pulse used in our TA experiments, and (b) the ~5 ns FWHM pulse used in our TRMC experiments. Despite relatively large quenching rate constants (see table S2) the charge yield attained is not significantly dependent on the pulse width due to the low excitation fluence (10^{12} photons/pulse/cm^2 — 10^{17} photons/pulse/cm^{-3})*

8. Supporting Information References

(1) Sisto, T. J.; Zhong, Y.; Zhang, B.; Trinh, M. T.; Miyata, K.; Zhong, X.; Zhu, X. Y.; Steigerwald, M. L.; Ng, F.; Nuckolls, C. Long, Atomically Precise Donor–Acceptor Cove-Edge Nanoribbons as Electron Acceptors. *Journal of the American Chemical Society* **2017,** *139*, 5648-5651.
(2) Peurifoy, S. R.; Castro, E.; Liu, F.; Zhu, X. Y.; Ng, F.; Jockusch, S.; Steigerwald, M. L.; Echegoyen, L.; Nuckolls, C.; Sisto, T. J. Three-Dimensional Graphene Nanostructures. *Journal of the American Chemical Society* **2018,** *140*, 9341-9345.
(3) Kang, H. S.; Sisto, T. J.; Peurifoy, S.; Arias, D. H.; Zhang, B.; Nuckolls, C.; Blackburn, J. L. Long-Lived Charge Separation at Heterojunctions between Semiconducting Single-Walled Carbon Nanotubes and Perylene Diimide Electron Acceptors. *The Journal of Physical Chemistry C* **2018,** *122*, 14150-14161.
(4) Ferguson, A. J.; Reid, O. G.; Nanayakkara, S. U.; Ihly, R.; Blackburn, J. L. Efficiency of Charge-Transfer Doping in Organic Semiconductors Probed with Quantitative Microwave and Direct-Current Conductance. *The Journal of Physical Chemistry Letters* **2018,** *9*, 6864-6870.
(5) Dowgiallo, A.-M.; Mistry, K. S.; Johnson, J. C.; Blackburn, J. L. Ultrafast Spectroscopic Signature of Charge Transfer between Single-Walled Carbon Nanotubes and C60. *ACS Nano* **2014,** *8*, 8573-8581.
(6) Guillot, S. L.; Mistry, K. S.; Avery, A. D.; Richard, J.; Dowgiallo, A.-M.; Ndione, P. F.; van de Lagemaat, J.; Reese, M. O.; Blackburn, J. L. Precision Printing and Optical Modeling of Ultrathin Swcnt/C60 Heterojunction Solar Cells. *Nanoscale* **2015,** *7*, 6556-6566.
(7) Reid, O. G.; Moore, D. T.; Li, Z.; Zhao, D.; Yan, Y.; Zhu, K.; Rumbles, G. Quantitative Analysis of Time-Resolved Microwave Conductivity Data. *Journal of Physics D: Applied Physics* **2017,** *50*, 493002.